Electrochemical treatment of butylated hydroxyanisole: Electrocoagulation versus advanced oxidation

Zhihong Ye, Enric Brillas, Francesc Centellas, Pere Lluís Cabot, Ignasi Sirés*

Laboratori d'Electroquímica dels Materials i del Medi Ambient, Departament de Química Física, Facultat de Química, Universitat de Barcelona, Martí i Franquès 1-11, 08028 Barcelona, Spain

Corresponding author: * i.sires@ub.edu (I. Sirés)

Abstract

This work compares the removal of butylated hydroxyanisole (BHA), a ubiquitous antioxidant in food and pharmaceuticals, from water either by electrocoagulation (EC) with an Fe|Fe cell or H_2O_2-based electrochemical advanced oxidation processes like electrochemical oxidation (EO-H_2O_2), electro-Fenton (EF) and photoelectro-Fenton (PEF) with an air-diffusion cathode. BHA degradation by EC was very poor, whereas the dissolved organic carbon (DOC) was more effectively abated in urban wastewater. The effect of pH, number of Fe|Fe pairs and current on the EC performance was examined. The additive was also slowly degraded by EO-H_2O_2 with a RuO_2-based or BDD anode in 50 mM Na_2SO_4 solution. In the simulated matrix, BHA decay by EO-H_2O_2 was substantially enhanced owing to active chlorine generation from anodic oxidation of Cl^-, whereas the $^\bullet$OH-mediated oxidation at the BDD surface accounted for DOC decay. In EF and PEF, the $^\bullet$OH produced in the bulk upgraded the mineralization, primordially using BDD. In rawurban wastewater at natural pH 7.9, the time course of BHA and DOC contents was affected by NOM oxidation, being accelerated in the order: EO-H_2O_2 < EF < PEF. The quickest decontamination of urban wastewater occurred in PEF at pH 3.0, because of the higher amounts of $^\bullet$OH in the bulk along with UVA photolysis.

Keywords: Butylated hydroxyanisole; Electrochemical advanced oxidation processes; Electrocoagulation; Industrial additives; Urban wastewater

1. Introduction

Butylated hydroxyanisole (BHA, $C_{11}H_{16}O_2$, M = 180.2 g mol^{-1}) is a synthetic phenolic antioxidant added to food, pharmaceuticals and cosmetics. It is widely used as industrial preservative since it delays or prevents the onset of lipid oxidation in such products, thereby ensuring their quantitative uptake into the body. BHA consists of a mixture of two liposoluble isomers, i.e., 2(3)-tert-butyl-4-hydroxyanisole [1,2], which can cause harmful effects on human health because of the potential formation of complexes with nucleic acids leading to DNA damage [2]. The Joint FAO/WHO Expert Committee on Food Additives (JECFA) limits the acceptable daily intake to 0.5 mg kg^{-1} [1,2]. In Europe, BHA is limited to 200 mg kg^{-1} on the fat content of products such as dehydrated soups and meat, gravies and bouillons [2]. Due to its frequent usage, it has been detected in rivers, groundwater and wastewater from various European and American countries, reaching up to 2 μg L^{-1} [1]. However, only some few works have reported the removal of BHA from water, focusing on UVC photoloysis [3] and its combination with ozone [3] or $S_2O_8^{2-}$ [4], ozonation [3,5] and chlorination [6]. These treatments yield stable by-products like 3-tert-butyl-4,5-dihydroxyanisole, tert-butyl-1,4-hydroquinone and hydroquinone [3,6], which should be completely destroyed because they are highly toxic. Investigation on other powerful advanced oxidation processes (AOPs), not tested for BHA so far, is thus needed. The oxidation ability of AOPs is based on the large production of reactive oxygen species (ROS) like hydroxyl radical ($^{\bullet}OH$), which reacts with most organics causing their mineralization [7-9].

Several electrochemical methods (EAOPs) have been recently developed as an alternative to remove organic pollutants from water [10-15]. The leading EAOP is electrochemical oxidation (EO), which involves the generation of adsorbed hydroxyl radical ($M(^{\bullet}OH)$) at the surface of an anode M, as follows [10,14,16,17]:

$$M + H_2O \rightarrow M(^{\bullet}OH) + H^+ + e^- \quad (1)$$

The oxidation power of M(•OH) directly depends on the anode nature. It has been found that non-active boron-doped diamond (BDD) thin-films give rise to the most powerful oxidant (BDD(•OH)) in inert electrolytes, because of its large O_2-evolution overpotential and quasi-free interaction between •OH and BDD surface [10,16,18]. In contrast, active electrodes like dimensionally stable anodes (DSA®) accumulate much smaller amounts of M(•OH) since this is quickly oxidized to the weaker oxidant MO [19,20]. In the presence of chloride, other powerful oxidants such as active chlorine (Cl_2/HClO/ClO^-) are also formed from reactions (2)-(4), depending on pH, competing with M(•OH) to react with organics [21,22].

$$2\,Cl^- \rightarrow Cl_2(aq) + 2e^- \quad (2)$$

$$Cl_2(aq) + H_2O \rightarrow HClO + Cl^- + H^+ \quad (3)$$

$$HClO \leftrightarrows ClO^- + H^+ \qquad pK_a = 7.54 \quad (4)$$

Setups that include an undivided cell equipped with a cathode like carbon felt [23-25], graphite [26], carbon-polytetrafluoroethylene (PTFE) in gas-diffusion mode [22,27-29], reticulated vitreous carbon [30], carbon nanotubes [31], carbon fiber [30,32] or BDD [33] allow the co-generation of weaker ROS such as H_2O_2 from O_2 reduction by reaction (5):

$$O_2(g) + 2H^+ + 2e^- \rightarrow H_2O_2 \quad (5)$$

This EAOP is known as EO with electrogenerated H_2O_2 (EO-H_2O_2). Under these conditions, addition of Fe^{2+} to the solution gives rise to electro-Fenton (EF) process [11,12,34]. In EF, homogeneous •OH are formed by Fenton's reaction (6), whose optimum pH is ca. 3, and Fe^{2+} can be regenerated upon Fe^{3+} reduction at the cathode. Organic pollutants can then be simultaneously attacked by both, M(•OH) at the anode surface and •OH in the bulk. The photoelectro-Fenton (PEF) process involves the additional exposure of the solution to UV light [11-13,27]. The incident photons can photoreduce $Fe(OH)^{2+}$, the predominant Fe(III) species in the bulk, via reaction (7), as well as photodecompose

77 photoactive intermediates like Fe(III) complexes with generated carboxylic acids according to
78 the general reaction (8).

79 $H_2O_2 + Fe^{2+} \rightarrow Fe^{3+} + {}^{\bullet}OH + OH^-$ (6)

80 $Fe(OH)^{2+} + h\nu \rightarrow Fe^{2+} + {}^{\bullet}OH$ (7)

81 $Fe(OOCR)^{2+} + h\nu \rightarrow Fe^{2+} + CO_2 + R^{\bullet}$ (8)

82 A more classical electrochemical technology for wastewater treatment, already
83 implemented in some companies, is electrocoagulation (EC). Its most characteristic feature is
84 the removal of colloidal and charged particles by adsorption onto the Fe(III) or Al(III)
85 hydroxides originated from the dissolution of Fe or Al anodes [35,36]. In the case of Fe, the
86 anode is oxidized to Fe^{2+} via reaction (9), which is further oxidized to insoluble $Fe(OH)_3$ by
87 O_2 gas according to reaction (10).

88 $Fe \rightarrow Fe^{2+} + 2\ e^-$ (9)

89 $4\ Fe^{2+} + 10\ H_2O + O_{2(g)} \rightarrow 4\ Fe(OH)_{3(s)} + 8\ H^+$ (10)

90 Although EC is considered a phase separation method, earlier work has shown that
91 neutral organic molecules can be attacked by active chlorine generated in the presence of Cl^-
92 from reactions (2)-(4) [37], eventually producing by-products that can also adsorb onto the
93 flocs formed along the treatment.

94 In this work, the performance of EC and EAOPs like EO-H_2O_2, EF and PEF to remove
95 BHA from different water matrices was compared. Main experiments were performed in
96 urban wastewater using an Fe anode in EC and a BDD or RuO_2-based one in EAOPs. The
97 role of the generated flocs, oxidizing agents and/or UVA irradiation was clarified by using a
98 50 mM Na_2SO_4 solution and a simulated matrix with similar ionic content to the urban
99 wastewater. The effect of several experimental parameters on BHA and dissolved organic
100 carbon (DOC) removals was examined for each treatment.

2. Materials and methods

2.1. Reagents

BHA (99% purity) was supplied by Sigma-Aldrich as a mixture of two isomers, 10% of 2-tert-butyl-4-hydroxyanisole and 90% of 3-tert-butyl-4-hydroxyanisole. The catalyst used for the EF and PEF runs was $FeSO_4 \cdot 7H_2O$ of analytical grade from J.T. Baker. Millipore Milli-Q water with resistivity > 18.2 MΩ cm was employed for the preparation of all synthetic solutions. The salts used as electrolytes and other chemicals used for analysis were of HPLC or analytical grade from Alfa Aesar, Panreac and Merck.

2.2. Aqueous matrices employed to perform the electrochemical treatments

The trials were carried out in three different aqueous matrices:

(i) Real wastewater, which corresponded to secondary clarifier effluent from a municipal wastewater treatment plant located in Gavà-Viladecans (Barcelona, Spain). The sample was preserved at 4 ºC before use. Its main characteristics were: pH = 7.9±0.3; specific conductivity = 2.19±0.11 mS cm^{-1}; DOC = 18.0±0.9 mg L^{-1}; cations: 328 mg L^{-1} Na^+, 49 mg L^{-1} K^+, 99 mg L^{-1} Ca^{2+}, 36 mg L^{-1} Mg^{2+}, 0.19 mg L^{-1} Fe^{2+} and 36.9 mg L^{-1} NH_4^+; and anions: 117 mg L^{-1} SO_4^{2-}, 480 mg L^{-1} Cl^-, 0.85 mg L^{-1} NO_3^- and 0.79 mg L^{-1} NO_2^-.

(ii) A simulated matrix that mimicked the main ionic content of the urban wastewater, but without its natural organic matter (NOM) components (primordially, soluble humic and fulvic acids). It was prepared in Milli-Q water by adding salts that accounted for 140 mg L^{-1} SO_4^{2-}, 405 mg L^{-1} Cl^-, 309 mg L^{-1} Na^+ and 52 mg L^{-1} K^+. The resulting pH was 5.9 and the specific conductivity was 1.79 mS cm^{-1}.

(iii) A 50 mM Na_2SO_4 solution in Milli-Q water at pH 5.9, with specific conductivity of 5.9 mS cm^{-1}, which was used for a more thorough comparison.

125 *2.3. Electrolytic systems*

126 The electrolytic experiments were carried out in an open, undivided glass cell containing
127 150 mL samples under vigorous stirring provided by a magnetic follower. The cell had a
128 double jacket for circulation of thermostated water at 35 °C.

129 For the EC trials, the anode and cathode were iron plates of 2.75 cm × 1.5 cm, 0.25 cm
130 thickness. One or two electrode pairs were placed alternately in parallel with 1.0 cm
131 separation. Before each run, the electrodes were cleaned with a 20% (v/v) H_2SO_4/water
132 mixture, rinsed with Milli-Q water and dried to constant weight.

133 For the EO-H_2O_2, EF and PEF treatments, the anode of 3 cm^2 area was either a RuO_2-
134 based plate (DSA®-Cl_2) purchased from NMT Electrodes (Pinetown, South Africa) or a BDD
135 thin-film on a Si wafer purchased from NeoCoat (La Chaux-de-Fonds, Switzerland). The
136 cathode was a 3 cm^2 carbon-PTFE air-diffusion electrode supplied by E-TEK (Division of De
137 Nora N.A., Inc.), mounted as reported before [20] and fed with air at 1 L min^{-1} to
138 continuously produce H_2O_2 from reaction (5). The interelectrode gap was close to 1.0 cm. The
139 electrodes were initially activated/cleaned under polarization in 50 mM Na_2SO_4 at 300 mA
140 for 180 min. The EF and PEF trials were performed in the presence of 0.50 mM Fe^{2+}, which is
141 the optimum content found for these treatments under the present conditions. The PEF assays
142 were ran by irradiation of the whole solution with a Philips TL/6W/08 fluorescent black light
143 blue tube, placed at 7 cm above its surface and emitting UVA light (320–400 nm, λ_{max}= 360
144 nm) with irradiance of 5 W m^{-2}, as detected with a Kipp & Zonen CUV 5 radiometer.

145 *2.4. Analytical methods*

146 Constant current electrolyses were made with an Amel 2053 potentiostat-galvanostat.
147 The electrical conductance was measured with a Metrohm 644 conductometer. The solution
148 pH was determined with a Crison GLP 22 pH-meter. The active chlorine concentration was
149 obtained by means of the *N*,*N*-diethyl-*p*-phenylenediamine colorimetric method using a

Shimadzu 1800 UV/Vis spectrophotometer at λ = 515 nm [38]. The concentration of anions and cations in the urban wastewater was obtained as described elsewhere [39].

Samples withdrawn from the treated aqueous matrices were microfiltered with 0.45 μm PTFE filters from Whatman before analysis. The BHA concentration was measured by reversed-phase HPLC using a Waters system, as described elsewhere [39,40]. The photodiode array detector was set at λ = 290 nm. The injected aliquot was 10 μL and the mobile phase was a 70:30 (v/v) mixture of acetonitrile and 10 mM KH_2PO_4 (pH 3.0) eluted at 1 mL min^{-1}. BHA appeared in the chromatograms at a retention time of 5.1 min.

The solution DOC was determined on a Shimadzu TOC-VCNS analyzer using the non-purgeable organic carbon method. Considering the following theoretical total mineralization reaction for BHA with a number of carbon atoms (*m*) of 11 and a number of exchanged electrons (*n*) of 56:

$$C_{11}H_{16}O_2 + 20\ H_2O \rightarrow 11\ CO_2 + 56\ H^+ + 56\ e^- \quad (11)$$

the mineralization current efficiency (MCE, in %) at each electrolysis time *t* (in h) was calculated from DOC decay ($\triangle$(DOC), in mg L^{-1}) at given current *I* (in mA) by Eq. (12) [41]:

$$\%\ \mathrm{MCE} = \frac{n\,F\,V\,\triangle(\mathrm{DOC})}{4.32\times10^7\,m\,I\,t} \times 100 \quad (12)$$

where *F* is the Faraday constant (96,485 C mol^{-1}), *V* is the solution volume (in L), and 4.32×10^7 is a conversion factor for units homogenization (3,600 s h^{-1} × 12,000 mg C mol^{-1}).

Each experiment to determine BHA and DOC decays was made in triplicate and average values are given along with the corresponding error bars (95% confidence intervals).

3. Results and discussion

3.1. Electrocoagulation of BHA in different aqueous matrices

Once the stability of the target pollutant in the whole pH range was verified, first assays were performed by treating 150 mL of 76 μM BHA. They were made in the simulated matrix or urban wastewater at their characteristic pH, applying 100 mA in an Fe|Fe cell for 60 min. In both cases, it was observed that the pH rose with electrolysis time up to a final value of 9.7 due to the excess of OH^- ions produced from cathodic water reduction, which occurred in concomitance with the Fe anode dissolution to Fe^{2+} via reaction (9).

Fig. 1a shows the change of the normalized BHA concentration during these experiments. As can be seen, the BHA content was finally reduced by 10.5% in the simulated matrix and 3.6% in urban wastewater. It is noticeable the faster removal during the first 5 min of electrolysis, which can be related to the quick adsorption of BHA onto the $Fe(OH)_3$ flocs produced, being much more remarkable in real wastewater. After that time, the partial redissolution of adsorbed BHA explains the increasing soluble content until the adsorption/desorption equilibrium was attained at about 25-30 min. The initially greater removal in urban wastewater suggests a strong influence of NOM components. They contributed to the entrapment of BHA, resulting in a larger adsorption, but at longer time the progressive cleavage of such components promoted the adsorption of resulting by-products over BHA on the $Fe(OH)_3$ flocs. As a result, the percentage of pollutant removal in real wastewater was lower. This explanation agrees with the normalized DOC decay in both media, as depicted in Fig. 1b. In the simulated matrix, the DOC profile was similar to BHA decay, with a final abatement of 10.2%. This suggests that BHA was the main organic adsorbed onto the hydroxides, with insignificant retention of its possible by-products such as those formed upon reaction with generated active chlorine [21]. The stability of these intermediates against coagulation justifies the appearance of a plateau. In contrast, in urban

wastewater, a more relevant DOC decay of 24.1% was achieved, which differs from 3.6% of BHA removal shown in Fig. 1a. This means that in the latter matrix the EC treatment mainly promoted the removal of NOM components, inhibiting that of BHA.

The adsorption of BHA was checked with another assay carried out with much higher pollutant content (1.50 mM) in the simulated matrix under comparable conditions. Fig. 1a and b evidences quite similar profiles for BHA and DOC decays with electrolysis time, being also analogous to those discussed above for 76 μM BHA. As the only difference, the minimum DOC content at 5 min was more pronounced at higher BHA concentration, which suggests that the amount of pollutant adsorbed onto $Fe(OH)_3$ is regulated by its content in the matrix.

The effect of pH, number of Fe|Fe pairs and applied current on the performance of the EC treatment of 76 μM BHA spiked into urban wastewater was subsequently assessed. Fig. S1a shows a small substrate removal at all pH values tested using one Fe|Fe pair at 100 mA, slightly increasing in the order: natural pH 5.9 (3.6%) < pH 11.0 (8.8%) < pH 3.0 (11.2%). The larger disappearance at pH 3.0 can be accounted for by the attack of active chlorine (Cl_2/HClO) [37], which causes the destruction of BHA. The potential contribution of adsorption on flocs can be practically discarded at pH 3.0, confirming the low content of $Fe(OH)_3$ at pH < 3.5. The better removal at pH 11.0 could then be associated with its enhanced adsorption because of the larger formation of such flocs in alkaline medium, along with a poor destruction by ClO^-, the weakest active chlorine species [21,37]. In contrast, at pH 5.9 the initial removal by adsorption was predominant, followed by greater desorption as compared to the other pH values. The same tendency can be observed in Fig. S1b for the corresponding normalized DOC content, being reduced by 24.1%, 27.8% and 33.1% at pH 5.9, 11.0 and 3.0, respectively, owing to the increasing coagulation of NOM components. It can then be inferred that, despite the smaller formation of $Fe(OH)_3$, pH 3.0 resulted optimal for the EC treatment of BHA due to the positive contribution of generated active chlorine.

220 However, all these results are indicative of a very poor BHA degradation during EC, since it
221 can only be hardly destroyed by small amounts of active chlorine produced.

222 A system with two Fe|Fe pairs placed alternately in monopolar parallel connection was
223 compared to the previous setup at natural pH 5.9 and 100 mA. Fig. S1a and b evidences larger
224 BHA and DOC decays using four electrodes, achieving 10.5% and 30.2%, respectively. This
225 can be related to the smaller current density applied to each anode since it: (i) increases the
226 current efficiency by maximizing the Fe dissolution over the H_2O oxidation, and (ii) allows a
227 more controlled release of Fe^{2+}, leading to a better formation and growth of hydroxides whose
228 final size enhances the adsorption of BHA and NOM.

229 Based on this result, the influence of the applied current was examined between 50 and
230 150 mA at natural pH using the two Fe|Fe pairs. Fig. 2a highlights a large enhancement of the
231 initial BHA removal during the first 5 min upon current increase, as expected by the greater
232 amounts of $Fe(OH)_3$ flocs formed with ability to cause a larger adsorption. This was
233 confirmed from the predominance of BHA adsorption over desorption at longer electrolysis
234 time, finally yielding 7.4%, 10.5% and 19.2% removal at 50, 100 and 150 mA, respectively.
235 The same tendency is shown in Fig. 2b, where DOC gradually disappears to attain removals
236 of 26.8%, 30.2% and 36.4%. A smaller relative removal of NOM was then obtained as current
237 was raised, due to the greater quantity of pollutants molecules adsorbed onto the more
238 numerous flocs formed.

239 Since EC did not allow a significant decontamination of urban wastewater spiked with
240 BHA, EAOPs were tested, as will be discussed in subsections below.

241 *3.2. Generation of active chlorine in synthetic aqueous media by EO*

242 Prior to the treatment of BHA in synthetic solutions, the ability of EO to accumulate
243 active chlorine in the bulk of electrolyzed solutions was analyzed. To do this, 150 mL of a
244 synthetic solution with 10 mM NaCl + 10 mM Na_2SO_4 at pH 5.9 were electrolyzed using a

cell with a RuO_2-based or BDD anode and an Al cathode at 150 mA for 300 min. This arrangement prevents the consumption of HClO by reaction with H_2O_2, which typically occurs when an air-diffusion cathode is utilized [21,37,39]. As can be seen in Fig. S2, Cl^- ion abatement reached 88.5% with BDD and only 14.9% with the RuO_2-based anode, since the former material favors reaction (3). Conversely, with BDD the active chlorine was only accumulated up to 0.56 mM at 90 min and disappeared at 300 min, whereas all the active chlorine generated at the RuO_2-based anode remained stable, reaching a final concentration of about 1.5 mM that equated the Cl^- content lost. The total removal of active chlorine using BDD can be accounted for by its well known conversion into ClO_3^- and ClO_4^- ions [42,43]. These findings indicate that, in the EAOPs, the competitive oxidation with active chlorine will be more remarkable using a RuO_2-based anode.

3.3. Degradation of BHA in 50 mM Na_2SO_4 solution and simulated matrix by EO-H_2O_2

First, 150 mL of 76 μM BHA in both media at natural pH 5.9 were treated by EO-H_2O_2 using a RuO_2-based or BDD anode, at 100 mA for 300 min. During these tests, the solution pH decreased slightly, probably due to the formation of acidic by-products [11-13].

Fig. 3a depicts a very slow decay of the pollutant concentration in 50 mM Na_2SO_4 solution, being degraded by 63.8% and 70.7% at the end of the treatment using the RuO_2-based and BDD anode, respectively. Under these conditions, BHA reacts with adsorbed M($^\bullet$OH) originated from reaction (1) and thus, the superiority of BDD agrees with the expected higher oxidation power of BDD($^\bullet$OH) as compared to RuO_2($^\bullet$OH) [10,16]. The concentration decays were analyzed using kinetic equations related to simple reaction orders, and excellent fits were obtained for a pseudo-first-order process, as shown in Fig. S3a. Alternatively, the very slow concentration decays in the EO-H_2O_2 processes could suggest the occurrence of a pseudo-zero-order kinetics. The apparent rate constants (k_1) along with the squared linear regression coefficients (R^2) are summarized in Table 1. This behavior can be

interpreted considering that a constant but small M(•OH) concentration attacks the pollutant once it arrives at the anode surface.

A very different trend can be observed in Fig. 3a in the simulated matrix, where the contaminant concentration fell very rapidly, practically independent of the anode nature, to be below the limit of quantification at about 30 min. From the good linear regressions (Fig. S3a), the k_1-values in the simulated matrix were 18.4-fold and 14.6-fold higher than those determined in 50 mM Na_2SO_4 solution using RuO_2-based and BDD anodes, respectively (see Table 1). The greater BHA decay in the simulated matrix can be accounted for by the attack of a low and constant active chlorine (HClO) concentration formed from reactions (3) and (4), whose action was much quicker than the simultaneous attack of M(•OH).

The mineralization role of generated oxidants was analyzed from the DOC abatement in each medium under the aforementioned conditions. Fig. 3b reveals a very small DOC abatement (< 5%) using a RuO_2-based anode (see Table 1). This means that RuO_2(•OH), alone in 50 mM Na_2SO_4 solution or in concomitance with active chlorine in the simulated matrix, is unable to destroy most of the intermediates (chlorinated and/or non-chlorinated) formed. In contrast, BDD(•OH) was much more powerful and thus, the use of BDD yielded 32.0% and 38.8% DOC decay in such media, respectively. Consequently, this anode is preferable in EO-H_2O_2, although only a partial mineralization was achieved, being slightly superior in the presence of Cl^- ion because BDD(•OH) is able to gradually mineralize chlorinated by-products. Accordingly, the MCE values determined for these experiments, illustrated in Fig. S4a, were below 0.15% using the RuO_2-based anode and between 1.1% and 1.3% with BDD, demonstrating the large recalcitrance of BHA by-products.

3.4. Degradation of BHA in synthetic aqueous solutions by EF and PEF

Once assessed the oxidation power of M(•OH) and active chlorine with BHA and its by-products as target molecules, the performance of •OH formed in the bulk from Fenton's

295 reaction (6) and UVA irradiation was analyzed under EF and PEF conditions in the presence
296 of 0.50 mM Fe^{2+} as catalyst. Fig. 4a shows a similar BHA decay in all cases, with total
297 removal in only 8 min. This is indicative of a very quick reaction of this pollutant with $^{\bullet}OH$,
298 much faster than the concomitant attack of M($^{\bullet}OH$) and active chlorine (see Fig. 3a). The
299 concentration decays of Fig. 4a obeyed to a pseudo-first-order reaction, as can be seen in Fig.
300 S3b, which means that BHA is removed by small and constant amounts of mixed oxidants,
301 i.e., RuO_2($^{\bullet}OH$) or BDD($^{\bullet}OH$), $^{\bullet}OH$ as the prevalent one, and active chlorine when Cl^- is
302 present. A look to Table 1 allows inferring that the k_1-values in EF and PEF were 4.1-4.7-fold
303 and 5.9-6.2-fold higher than those found in EO-H_2O_2, respectively, regardless of the anode
304 employed. The slightly faster BHA decay in PEF can be related to its oxidation by the
305 additional $^{\bullet}OH$ amount induced by photoreduction reaction (7).

306 A surprising result was obtained for the mineralization by EF process with the RuO_2-
307 based anode in the simulated matrix, as can be observed in Fig. 4b. DOC was abated by less
308 than 6%, meaning that most of the by-products cannot be transformed into CO_2 upon
309 combined action of RuO_2($^{\bullet}OH$), active chlorine and $^{\bullet}OH$. In contrast, the analogous treatment
310 under PEF conditions yielded 51.3% DOC removal at 300 min (see Fig. 4b and Table 1), as
311 expected if a large quantity of photoactive by-products were generated and mineralized by
312 UVA radiation. Using BDD anode, Fig. 4b shows a gradual drop of DOC in EF and PEF,
313 achieving 66.5% and 81.2% removal (see Table 1). This confirms the very effective oxidation
314 of by-products by BDD($^{\bullet}OH$) in EF. In turn, this yields photoactive by-products that can be
315 more quickly photolyzed by UVA photons. Nevertheless, low MCE were determined in all
316 these Fenton-based treatments (see Fig. S4b), with a final value of 2.8% for the most powerful
317 treatment, i.e., PEF with BDD.

318 The final low MCE values in all the EAOPs are not surprising, because it is well known
319 that their efficiency diminishes largely as the organic load becomes smaller [10-15]. To show

this feature for BHA removal in the simulated matrix, an additional trial was performed by treating 150 mL of a highly concentrated solution (1.50 mM BHA) with 0.50 mM Fe^{2+} by PEF using a BDD/air-diffusion cell at 100 mA. A fast DOC abatement under these conditions can be seen in Fig. 5a, where 88.2% mineralization is reached at 360 min. Fig. 5b illustrates the MCE-time plot for this assay. An initial rise up to a 164.2% at 60 min can be observed, whereupon it dropped drastically down to 50.1%. This means that increasing contents of easy-to-mineralize by-products are formed at the beginning of PEF, whereas the generation of more recalcitrant molecules along with the reduction of the organic matter content cause the progressive MCE decay at long time [10]. Note that theoretical MCE values greater than 100% are feasible in this system, since oxidants are generated not only at the anode but also from H_2O_2 produced at the cathode.

3.5. Degradation of BHA in urban wastewater by EAOPs

The study of BHA removal by EAOPs was extended to urban wastewater as matrix by spiking this compound at 76 μM. First, 150 mL of the prepared solutions were treated at natural pH 7.9 at 100 mA for 300 min, with addition of Fe^{2+} as catalyst in EF and PEF. Fig. 6a illustrates the occurrence of a rapid BHA concentration abatement in all the EAOPs, with total removal at about 30 min. Hence, the disappearance in EO-H_2O_2 was somewhat slower to that described in the simulated matrix (see Fig. 3a), but much more difficult in the case of EF and PEF (see Fig. 4a). This slower decay in urban wastewater can be accounted for by the parallel attack of generated oxidants onto NOM components. The k_1-values for these trials are collected in Table 1, as determined from the kinetic analysis depicted in Fig. S3c. They highlight an increasing relative oxidation in the order: EO-H_2O_2 < EF < PEF, always being superior for the BDD anode. This trend is expected because BDD($^{\bullet}$OH) has higher oxidation power than RuO_2($^{\bullet}$OH). The attack of these species and active chlorine onto BHA in EO-H_2O_2 is reinforced by $^{\bullet}$OH formed from Fenton's reaction (6) in EF and, to a larger extent, by

additional •OH produced from photolytic reaction (7) in PEF. Note that the k_1-values for EO-H_2O_2 in urban wastewater were halved as compared to the simulated matrix (see Table 1), as expected if some of the M(•OH) and active chlorine react with NOM. In contrast, the data of Table 1 reveal a significant decrease of k_1 between 4.4-fold and 6.0-fold for the EF and PEF treatments in urban wastewater. This can be due to the smaller •OH production at its natural pH 7.9, if compared to the simulated matrix at pH 5.9 [11-13], along with the consumption of part of this radical by reaction with NOM.

Fig. 6b shows surprising profiles for DOC decays during the above experiments when a RuO_2-based anode was employed. As can be seen, the urban wastewater contaminated with BHA was very poorly decontaminated, attaining 10.4% as maximal (PEF process, see Table 1). This differs from the PEF behavior found in the simulated matrix, where DOC was reduced by 51.3% under comparable conditions (see Fig. 4b and Table 1). This agrees with the low •OH production at pH 7.9, inhibiting to a large extent the generation of photoactive intermediates that could have been removed by UVA light. This fact was confirmed from the DOC abatement using the BDD anode. Fig. 6b depicts a quite similar mineralization rate using this anode in all processes, slightly increasing as EO-H_2O_2 < EF < PEF (see also Table 1). This means that the main oxidant of BHA by-products and NOM is BDD(•OH) in all these treatments, with much smaller participation of •OH, active chlorine and UVA light. Comparison of Fig. 4b and 6b, as well as data of Table 1, allows inferring that the percentage of DOC decay was greater in urban wastewater for EO-H_2O_2, but superior in the simulated matrix for EF and PEF. However, since the initial DOC was much greater in urban wastewater (28 mg C L^{-1} vs. 10 mg C L^{-1}), a larger amount of organic carbon was always removed from the real matrix. This informs about the excellent ability of the EAOPs with a BDD anode to mineralize the NOM of urban wastewater at natural pH.

To better understand the oxidative role of •OH in EF and PEF, the comparative treatments of 76 μM BHA in urban wastewater with 0.50 mM Fe^{2+} were carried out at pH 3.0, where the rate of Fenton's reaction (6) becomes optimal [11-13]. Operating at 100 mA, Fig. 7a highlights a very fast removal of the pollutant, which disappeared in 4-6 min in all cases. These decays were much more rapid than in the analogous EF and PEF performed in the simulated matrix at pH 5.9 (see Fig. 4a), which corroborates the quick reaction of BHA with generated •OH in the bulk. When DOC removal was determined, a very poor mineralization was obtained again using the RuO_2-based anode (see Fig. 7b), although superior to that found at natural pH 7.9. Thus, for the powerful PEF, DOC was reduced by 23.7% at pH 3.0 vs. 10.4% at pH 7.9 (see Table 1). This suggests that the oxidation of BHA and NOM by •OH enhances the formation of photoactive intermediates that can be destroyed by UVA light. Fig. 7b also shows the beneficial use of BDD anode due to the pre-eminent attack of BDD(•OH), since 47.8% and 65.8% DOC abatements were obtained after 300 min of EF and PEF, respectively. The latter photoassisted Fenton-based method with BDD is then the best EAOP for BHA and/or NOM mineralization in a simulated matrix and urban wastewater within all the range.

To end, the high oxidation power of the above PEF process with BDD at pH 3.0 was assessed by prolonging the electrolysis time until almost total mineralization was achieved. Fig. 8 evidences that 97.0% of DOC removal was attained after 660 min of this treatment at 100 mA, as expected if the simultaneous action of BDD(•OH), active chlorine, •OH and UVA radiation can effectively destroy all the organic molecules contained in urban wastewater.

4. Conclusions

EC is not a convenient technology to remove BHA from water, as demonstrated with an Fe|Fe cell from the poor pollutant and DOC abatements in different aqueous media. The

adsorption of BHA onto $Fe(OH)_3$ flocs was relatively high within the first minutes, but at longer time it underwent a progressive redissolution. The best results were obtained at pH 3.0 due to the simultaneous oxidation with generated active chlorine. The use of several Fe|Fe pairs and higher current promoted a larger coagulation. The treatment of BHA in a 50 mM Na_2SO_4 solution by EO-H_2O_2 revealed a slow pollutant abatement using RuO_2-based and BDD anodes, but with much greater mineralization rate using the latter anode due to the higher oxidation power of BDD($^\bullet$OH). In a simulated matrix, the oxidation of BHA by active chlorine enhanced its removal in EO-H_2O_2, but BDD($^\bullet$OH) had the pre-eminent role during DOC abatement. The same effect was found during EF and PEF treatments in the simulated matrix, where the production of $^\bullet$OH favored the BHA decay and, to a smaller extent, its mineralization, always being BDD the most suitable anode. The degradation profiles in urban wastewater at natural pH 7.9 spiked with BHA confirmed the superiority of PEF with BDD, since the RuO_2-based anode was unable to mineralize BHA, NOM and all by-products. The quicker removals in urban wastewater at pH 3.0 confirmed the important role of $^\bullet$OH in the bulk, favoring the formation of photoactive intermediates that were more rapidly photodecomposed by UVA photons. Almost total mineralization with 97.0% DOC removal was achieved at pH 3.0 in PEF with BDD after 660 min at 100 mA.

Acknowledgements

The authors thank financial support from project CTQ2016-78616-R (AEI/FEDER, EU) and PhD scholarship awarded to Z.H. Ye (State Scholarship Fund, CSC, China).

References

[1] K.H.G. Freitas, O. Fatibello-Filho, Simultaneous determination of butylated hydroxyanisole (BHA) and butylated hydroxytoluene (BHT) in food samples using a

carbon composite electrode modified with $Cu_3(PO_4)_2$ immobilized in polyester resin, Talanta 81 (2010) 1102-1108.

[2] F. Shahidi, P. Ambigaipalan, Phenolics and polyphenolics in foods, beverages and spices: Antioxidant activity and health effects –A review, J. Funct. Foods 18 (2015) 820-897.

[3] T.K. Lau, W. Chu, N. Graham, Reaction pathways and kinetics of butylated hydroxyanisole with UV, ozonation, and UV/O_3 processes, Water Res. 41 (2007) 765-774.

[4] T.K. Lau, W. Chu, N.J.D. Graham, The aqueous degradation of butylated hydroxyanisole by UV/$S_2O_8^{2-}$: Study of reaction mechanisms via dimerization and mineralization, Environ. Sci. Technol. 41 (2007) 613-619.

[5] W. Chu, T.K. Lau, Ozonation of endocrine disrupting chemical BHA under the suppression effect by salt additive-with and without H_2O_2, J. Hazard. Mater. 144 (2007) 249-254.

[6] R. Rodil, J.B. Quintana, R. Cela, Oxidation of synthetic phenolic antioxidants during water chlorination, J. Hazard. Mater. 199-200 (2012) 73-81.

[7] M.A. Oturan, J.-J. Aaron, Advanced oxidation processes in water/wastewater treatment: principles and applications. A review, Crit. Rev. Environ. Sci. Technol. 44 (2014) 2577-2641.

[8] M. Antonopoulou, E. Evgenidou, D. Lambropoulou, I. Konstantinou, A review on advanced oxidation processes for the removal of taste and odor compounds from aqueous media, Water Res. 53 (2015) 215-234.

[9] G. Lofrano, R. Pedrazzani, G. Libralato, M. Carotenuto, Advanced oxidation processes for antibiotics removal: A review, Curr. Org. Chem. 21 (2017) 1-14.

440 [10] M. Panizza, G. Cerisola, Direct and mediated anodic oxidation of organic pollutants,
441 Chem. Rev. 109 (2009) 6541-6569.
442 [11] E. Brillas, I. Sirés, M.A. Oturan, Electro-Fenton process and related electrochemical
443 technologies based on Fenton's reaction chemistry, Chem. Rev. 109 (2009) 6570-6631.
444 [12] I. Sirés, E. Brillas, M.A. Oturan, M.A. Rodrigo, M. Panizza, Electrochemical advanced
445 oxidation processes: Today and tomorrow, Environ. Sci. Pollut. Res. 21 (2014) 8336-
446 8367.
447 [13] C.A. Martínez-Huitle, M.A. Rodrigo, I. Sirés, O. Scialdone, Single and coupled
448 electrochemical processes and reactors for the abatement of organic water pollutants: A
449 critical review, Chem. Rev. 115 (2015) 13362-13407.
450 [14] H. Särkkä, A. Bhatnagar, M. Sillanpää, Recent developments of electro-oxidation in
451 water treatment - A review, J. Electroanal. Chem. 754 (2015) 46-56.
452 [15] F.C. Moreira, R.A.R. Boaventura, E. Brillas, V.J.P. Vilar, Electrochemical advanced
453 oxidation processes: A review on their application to synthetic and urban wastewaters,
454 Appl. Catal. B: Environ. 202 (2017) 217-261.
455 [16] F. Bonfatti, S. Ferro, F. Lavezzo, M. Malacarne, G. Lodi, A. De Battisti,
456 Electrochemical incineration of glucose as a model organic substrate. I. Role of the
457 electrode material, J. Electrochem. Soc. 146 (1999) 2175-2179.
458 [17] B. Boye, P.A. Michaud, B. Marselli, M.M. Dieng, E. Brillas, C. Comninellis, Anodic
459 oxidation of 4-chlorophenoxyacetic acid on synthetic boron-doped diamond electrodes,
460 New Diamond Front. Carbon Technol. 12 (2002) 63-72.
461 [18] P. Cañizares, R. Paz, C. Sáez, M.A. Rodrigo, Electrochemical oxidation of alcohols and
462 carboxylic acids with diamond anodes. A comparison with other advanced oxidation
463 processes, Electrochim. Acta 53 (2008) 2144-2153.

[19] O. Scialdone, A. Galia, S. Randazzo, Oxidation of carboxylic acids in water at IrO_2-Ta_2O_5 and boron doped diamond anodes, Chem. Eng. J. 174 (2011) 266-274.

[20] J.R. Steter, E. Brillas, I. Sirés, On the selection of the anode material for the electrochemical removal of methylparaben from different aqueous media, Electrochim. Acta 222 (2016) 1464-1474.

[21] A. Thiam, M. Zhou, E. Brillas, I. Sirés, Two-step mineralization of Tartrazine solutions: Study of parameters and by-products during the coupling of electrocoagulation with electrochemical advanced oxidation processes, Appl. Catal. B: Environ. 150-151 (2014) 116-125.

[22] J.R. Steter, E. Brillas, I. Sirés, Solar photoelectro-Fenton treatment of a mixture of parabens spiked into secondary treated wastewater effluent at low input current, Appl. Catal. B: Environ. 224 (2018) 410-418.

[23] A. Dirany, I. Sirés, N. Oturan, A. Özcan, M.A. Oturan, Electrochemical treatment of the antibiotic sulfachloropyridazine: kinetics, reaction pathways, and toxicity evolution, Environ. Sci. Technol. 46 (2012) 4074-4082.

[24] A. El-Ghenymy, R.M. Rodríguez, E. Brillas, N. Oturan, M.A. Oturan, Electro-Fenton degradation of the antibiotic sulfanilamide with Pt/carbon-felt and BDD/carbon-felt cells. Kinetics, reaction intermediates, and toxicity assessment, Environ. Sci. Pollut. Res. 21 (2014) 8368-8378.

[25] M.S. Yahya, N. Oturan, K. El Kacemi, M. El Karbane, C.T. Aravindakumar, M.A. Oturan, Oxidative degradation study on antimicrobial agent ciprofloxacin by electro-Fenton process: Kinetics and oxidation products, Chemosphere 117 (2014) 447-454.

[26] O. Scialdone, E. Corrado, A. Galia, I. Sirés, Electrochemical processes in macro and microfluidic cells for the abatement of chloroacetic acid from water, Electrochim. Acta 132 (2014) 15-24.

[27] A. Bedolla-Guzman, I. Sirés, A. Thiam, J.M. Peralta-Hernández, S. Gutiérrez-Granados, E. Brillas, Application of anodic oxidation, electro-Fenton and UVA photoelectro-Fenton to decolorize and mineralize acidic solutions of Reactive Yellow 160 azo dye, Electrochim. Acta 206 (2016) 307-316.

[28] A. Galia, S. Lanzalaco, M.A. Sabatino, C. Dispenza, O. Scialdone, I. Sirés, Crosslinking of poly(vinylpyrrolidone) activated by electrogenerated hydroxyl radicals: A first step towards a simple and cheap synthetic route of nanogel vectors, Electrochem. Commun. 62 (2016) 64-68.

[29] S. Lanzalaco, I. Sirés, M.A. Sabatino, C. Dispenza, O. Scialdone, A. Galia, Synthesis of polymer nanogels by electro-Fenton process: investigation of the effect of main operation parameters, Electrochim. Acta 246 (2017) 812-822.

[30] B. Ramírez-Pereda, A. Álvarez-Gallegos, J.G. Rangel-Peraza, Y.A. Bustos-Terrones, Kinetics of Acid Orange 7 oxidation by using carbon fiber and reticulated vitreous carbon in an electro-Fenton process, J. Environ. Manage. 213 (2018) 279-287.

[31] A. Khataee, A. Akbarpour, B. Vahi, Photoassisted electrochemical degradation of an azo dye using Ti/RuO_2 anode and carbon nanotubes containing gas-diffusion cathode, J. Taiwan Inst. Chem. Eng. 45 (2014) 930-936.

[32] A. Wang, J. Qu, H. Liu, J. Ru, Mineralization of an azo dye Acid Red 14 by photoelectro-Fenton process using an activated carbon fiber cathode, Appl. Catal. B: Environ. 84 (2008) 393-399.

[33] K. Cruz-González, O. Torres-López, A. García-León, E. Brillas, A. Hernández-Ramírez, J.M. Peralta-Hernández, Optimization of electro-Fenton/BDD process for decolorization of a model azo dye wastewater by means of response surface methodology, Desalination 286 (2012) 63-68.

513 [34] M. Panizza, M.A. Oturan, Degradation of Alizarin Red by electro-Fenton process
514 using a graphite-felt cathode, Electrochim. Acta 56 (2011) 7084-7087.
515 [35] M.A. Sandoval, R. Fuentes, J.L. Nava, I. Rodríguez, Fluoride removal from
516 drinking water by electrocoagulation in a continuous filter press reactor coupled to
517 a flocculator and clarifier, Sep. Purif. Technol. 134 (2014) 163-170.
518 [36] H. Lin, Y. Wang, J. Niu, Z. Yue, Q. Huang, Efficient sorption and removal of
519 perfluoroalkyl acids (PFAAs) from aqueous solution by metal hydroxides generated in
520 situ by electrocoagulation, Environ. Sci. Technol. 49 (2015) 10562-10569.
521 [37] E. Bocos, E. Brillas, M.A. Sanromán, I. Sirés, Electrocoagulation: Simply a phase
522 separation technology? The case of bronopol compared to its treatment by EAOPs,
523 Environ. Sci. Technol. 50 (2016) 7679-7686.
524 [38] APWA, AWWA, WEF, Standard Methods for the Examination of Water and
525 Wastewater, 21st Ed. Method Number 4500-Cl Chlorine (residual)–G. DPD
526 Colorimetric Method, American Public Health Association, Washington D.C., 2005, pp.
527 4-67 and 4-68.
528 [39] C. Ridruejo, C. Salazar, P.L. Cabot, F. Centellas, E. Brillas, I. Sirés, Electrochemical
529 oxidation of anesthetic tetracaine in aqueous medium. Influence of the anode and matrix
530 composition, Chem. Eng. J. 326 (2017) 811-819.
531 [40] R. Salazar, E. Brillas, I. Sirés, Finding the best Fe^{2+}/Cu^{2+} combination for the solar
532 photoelectro-Fenton treatment of simulated wastewater containing the industrial textile
533 dye Disperse Blue 3, Appl. Catal. B: Environ. 115-116 (2012) 107-116.
534 [41] E.J. Ruiz, A. Hernández-Ramírez, J.M. Peralta-Hernández, C. Arias, E. Brillas,
535 Application of solar photoelectro-Fenton technology to azo dyes mineralization: Effect
536 of current density, Fe^{2+} and dye concentration, Chem. Eng. J. 171 (2011) 385-392.

[42] D.K. Hubler, J.C. Baygents, B.P. Chaplin, J. Farrell, Understanding chlorite, chlorate and perchlorate formation when generating hypochlorite using boron doped diamond film electrodes, ECS Trans. 58 (2014) 21-32.

[43] H. Zöllig, A. Remmele, C. Fritzsche, E. Morgenroth, K.M. Udert, Formation of chlorination byproducts and their emission pathways in chlorine mediated electro-oxidation of urine on active and nonactive type anodes, Environ. Sci. Technol. 49 (2015) 11062-11069.

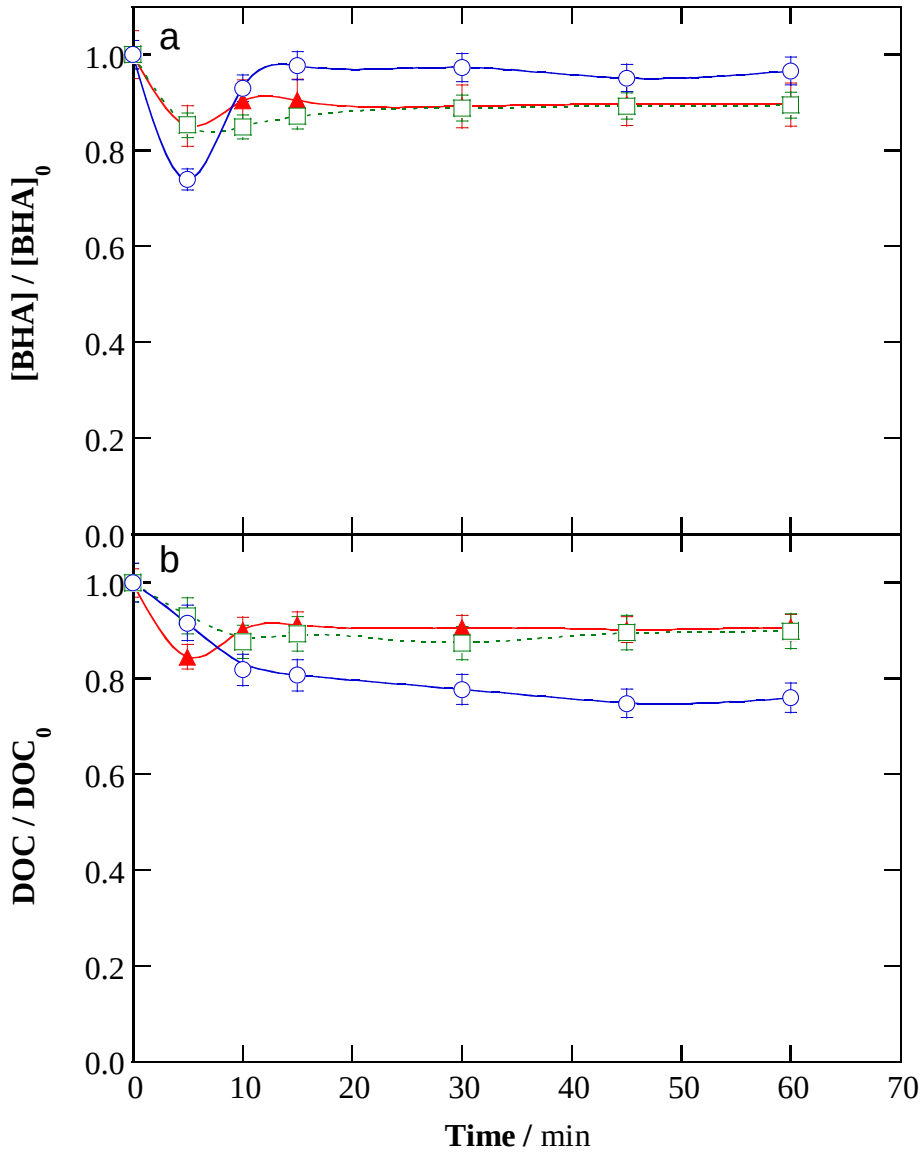

Fig. 1. Time course of the normalized (a) pollutant concentration and (b) dissolved organic carbon (DOC) for the electrocoagulation (EC) of 150 mL of (▲) 200 mg C L^{-1} (1.50 mM BHA) and (□,○) 10 mg C L^{-1} (76 μM BHA) in (▲,□) simulated matrix at natural pH 5.9 and (○) urban wastewater at natural pH 7.9, at 35 ºC using an Fe|Fe pair at 100 mA.

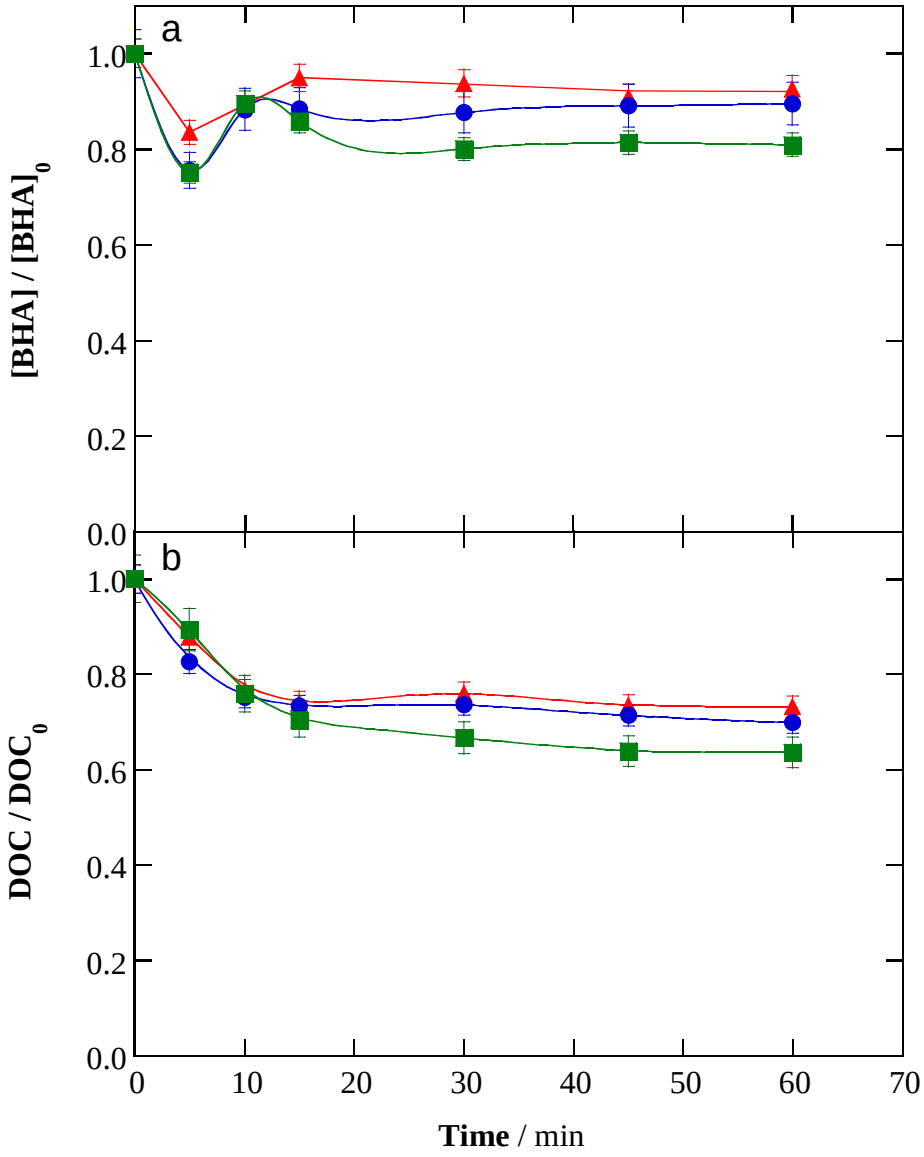

Fig. 2. Variation of normalized (a) pollutant concentration and (b) DOC with electrolysis time for the EC of 150 mL of solutions containing 10 mg C L^{-1} (76 μM BHA) in urban wastewater at natural pH 7.9 and 35 ºC using two Fe|Fe pairs at a current of: (▲) 50 mA, (●) 100 mA and (■) 150 mA.

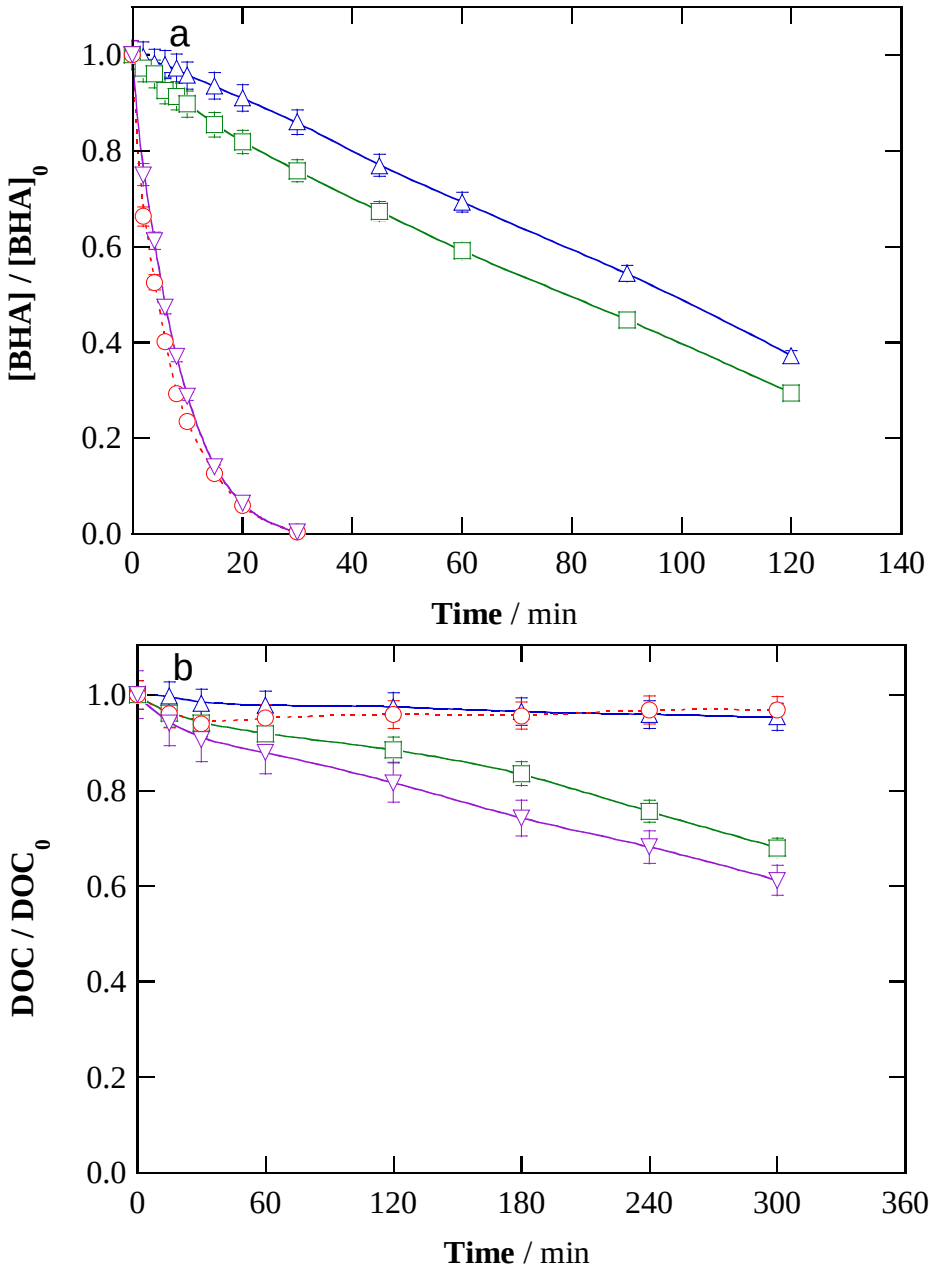

Fig. 3. Normalized (a) pollutant concentration and (b) DOC decays vs. electrolysis time for EO-H_2O_2 treatment of 150 mL of solutions containing 10 mg C L^{-1} (76 μM BHA) at pH 5.9 and 35 ºC using a cell with a 3 cm^2 air-diffusion cathode. Aqueous matrix: (△,□) 50 mM Na_2SO_4 and (○,▽) simulated matrix. Anode: 3 cm^2 (△,○) RuO_2-based and (□,▽) BDD. Applied current: 100 mA.

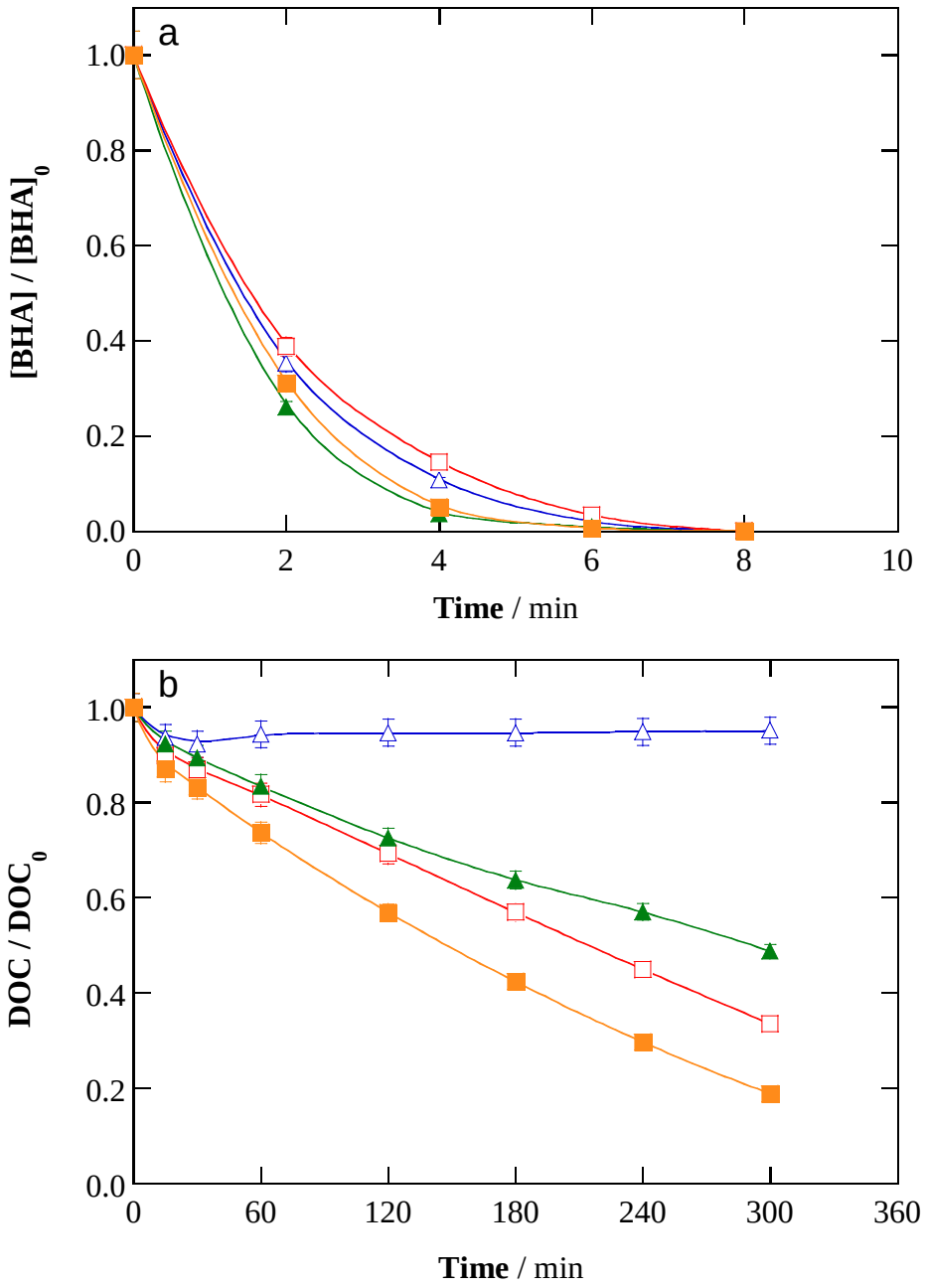

Fig. 4. Change of normalized (a) pollutant concentration and (b) DOC with electrolysis time for the treatment of 150 mL of 10 mg C L^{-1} (76 μM BHA) in a simulated matrix with 0.50 mM Fe^{2+} at pH 5.9 and 35 ºC using a cell with an air-diffusion cathode. Method: (△,□) Electro-Fenton (EF) and (▲,■) photoelectro-Fenton (PEF) under UVA irradiation with a 6 W lamp. Anode: (△,▲) RuO_2-based and (□,■) BDD. Applied current: 100 mA.

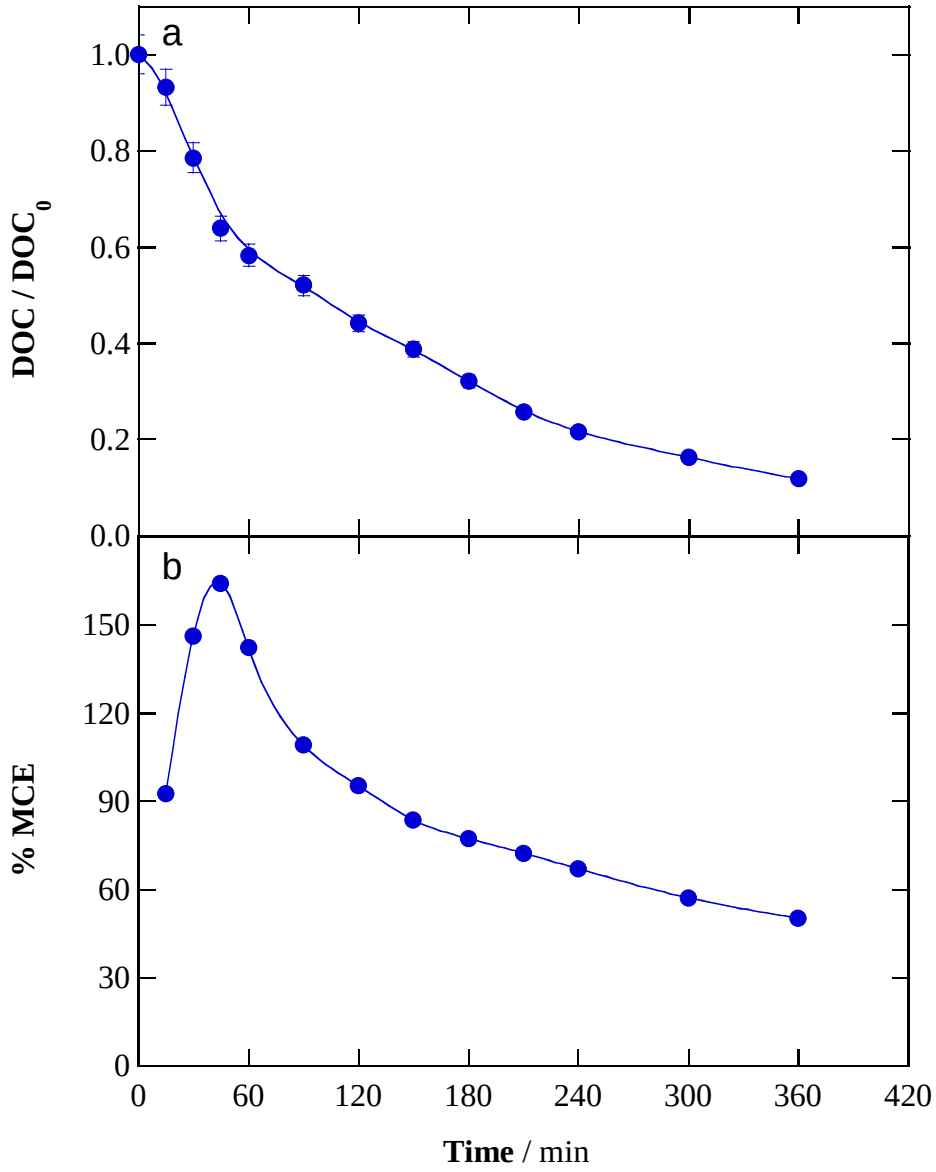

Fig. 5. Time course of the (a) normalized DOC and (b) mineralization current efficiency for the PEF degradation of 150 mL of 200 mg C L^{-1} (1.50 mM BHA) in a simulated matrix with 0.50 mM Fe^{2+} at pH 5.9 and 35 ºC using a BDD/air-diffusion cell at 100 mA.

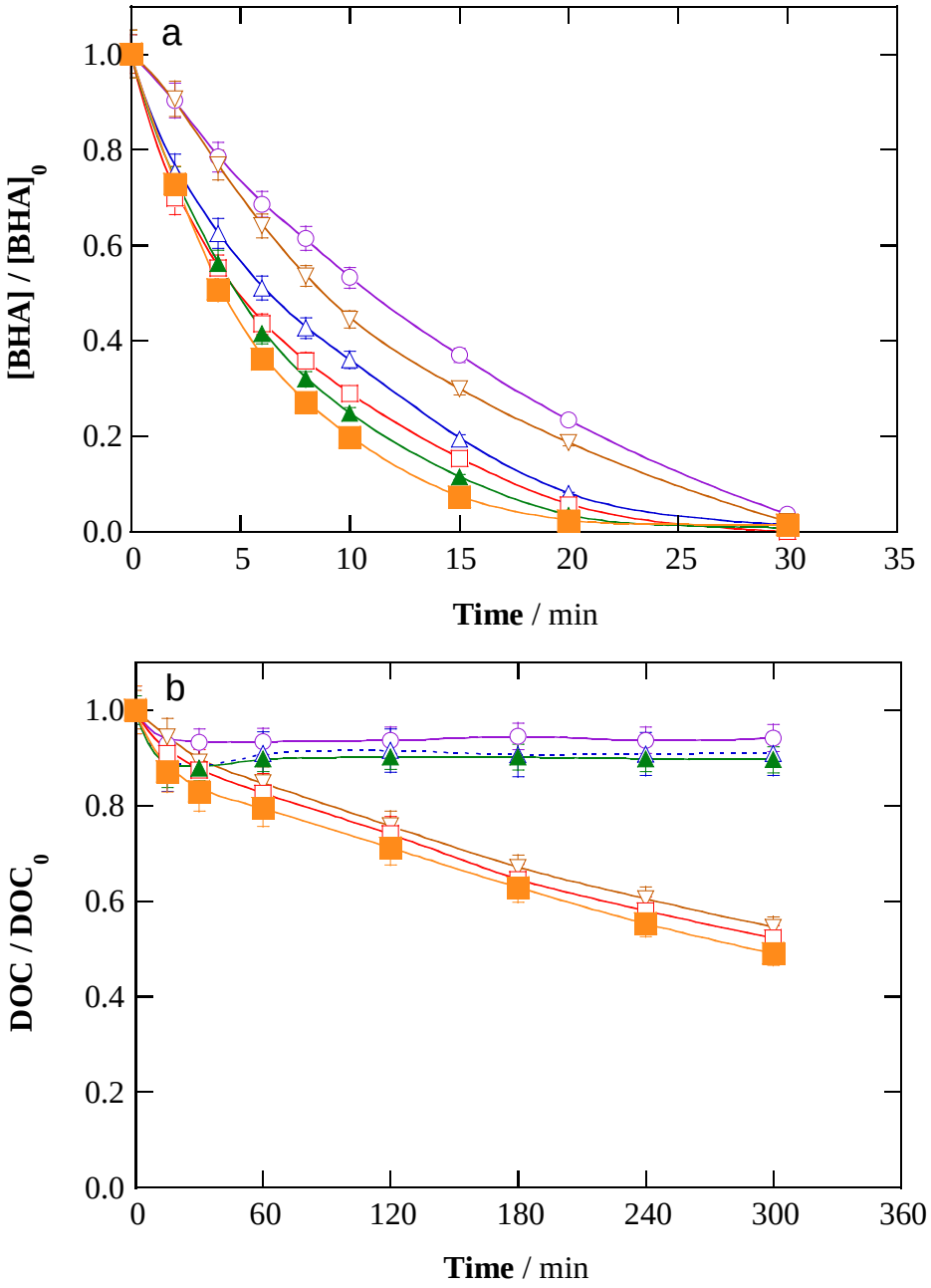

Fig. 6. Normalized (a) pollutant concentration and (b) DOC decays vs. electrolysis time for the treatment of 150 mL of 76 μM BHA, spiked into urban wastewater (total DOC of 28 mg L^{-1}) at natural pH 7.9 and 35 ºC using a cell with an air-diffusion cathode. Method: (○,▽) EO-H_2O_2, (△,□) EF with 0.50 mM Fe^{2+} and (▲,■) PEF with 0.50 mM Fe^{2+} and 6-W UVA lamp. Anode: (○,△,▲) RuO_2-based and (▽,□,■) BDD. Applied current: 100 mA.

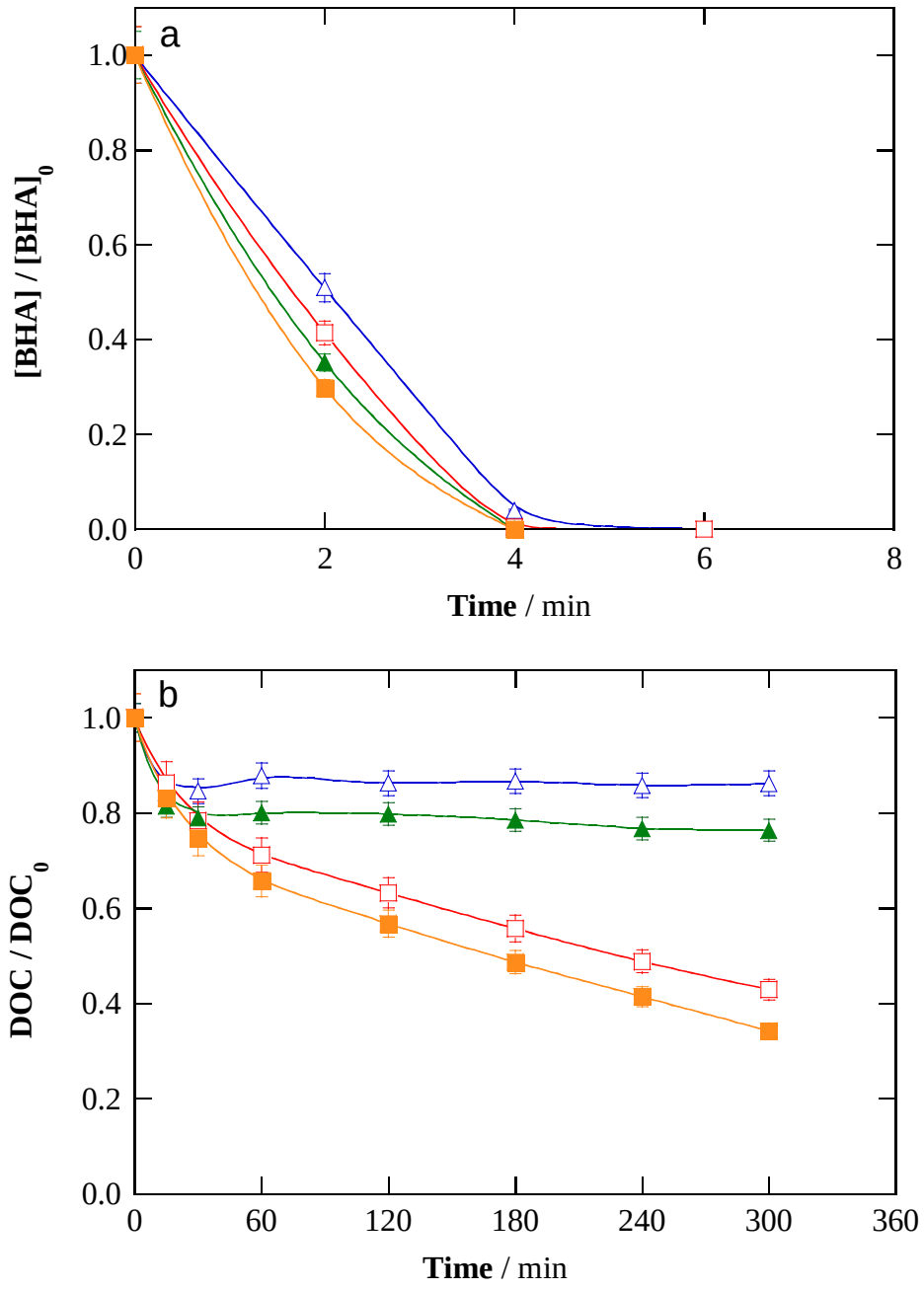

Fig. 7. Variation of normalized (a) pollutant concentration and (b) DOC with electrolysis time for the degradation of 150 mL of 76 μM BHA, spiked into urban wastewater (total DOC of 28 mg L^{-1}) with 0.50 mM Fe^{2+} at natural pH 3.0 and 35 ºC using a cell with an air-diffusion cathode by applying 100 mA. Method: (△,□) EF and (▲,■) PEF. Anode: (△,▲) RuO_2-based and (□,■) BDD.

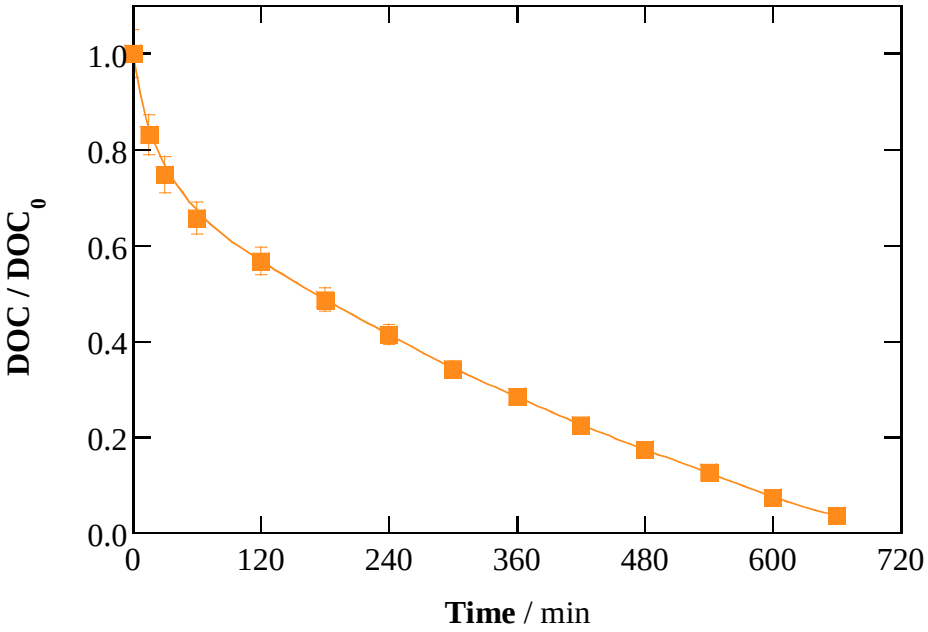

Fig. 8. Change of normalized DOC with electrolysis time for the PEF treatment of 150 mL of 10 mg C L^{-1} (76 μM BHA), spiked into urban wastewater with 0.50 mM Fe^{2+} at pH 3.0 and 35 ºC using a BDD/air-diffusion cell at 100 mA.

Table 1. Pseudo-first-order rate constant for BHA degradation along with the corresponding *R*-square and selected percentage of DOC removal, as determined for the degradation of 150 mL of 10 mg C L^{-1} (76 μM BHA) in different water matrices and pH values at 35 ºC by various EAOPs using a cell with an air-diffusion cathode at 100 mA.

Method	Anode	pH	k_1 (min^{-1})	R^2	% DOC removal at 300 min
50 mM Na_2SO_4 solution					
EO-H_2O_2	RuO_2-based	5.9	7.6×10^{-3}	0.987	4.6
	BDD	5.9	9.6×10^{-3}	0.992	32.0
Simulated matrix					
EO-H_2O_2	RuO_2-based	5.9	0.14	0.997	3.3
	BDD	5.9	0.14	0.996	38.8
EF[a]	RuO_2-based	5.9	0.66	0.984	5.0
	BDD	5.9	0.57	0.985	66.5
PEF[a,b]	RuO_2-based	5.9	0.82	0.995	51.3
	BDD	5.9	0.87	0.986	81.2
Urban wastewater[c]					
EO-H_2O_2	RuO_2-based	7.9	7.2×10^{-2}	0.993	5.9
	BDD	7.9	8.5×10^{-2}	0.998	45.5
EF[a]	RuO_2-based	3.0	0.34[d]	-	13.8
	BDD	3.0	0.44[d]	-	57.1
	RuO_2-based	7.9	0.11	0.993	9.2
	BDD	7.9	0.13	0.995	47.8
PEF[a,b]	RuO_2-based	3.0	0.53[d]	-	23.7
	BDD	3.0	0.61[d]	-	65.8
	RuO_2-based	7.9	0.16	0.993	10.4
	BDD	7.9	0.19	0.994	51.0

[a] With 0.50 mM Fe^{2+} as catalyst

[b] Under UVA irradiation

[c] Total initial DOC: 28 mg C L^{-1}

[d] Estimated as average value within the first 2 min of electrolysis